HHS Public Access

Author manuscript

Heart Rhythm. Author manuscript; available in PMC 2022 February 03.

Published in final edited form as:

Heart Rhythm. 2022 February ; 19(2): 281–292. doi:10.1016/j.hrthm.2021.10.005.

Disruption of protein quality control of the human *ether-à-go-go related* gene K^+ channel results in profound long QT syndrome

Hannah A. Ledford, PhD[*,1], **Lu Ren, MD, PhD**[*,1], **Phung N. Thai, PhD**[*], **Seojin Park, PhD**[*,†], **Valeriy Timofeyev, PhD**[*], **Padmini Sirish, PhD**[*,‡], **Wilson Xu, BS**[*], **Aiyana M. Emigh, BS**[§], **James R. Priest, MD**[‖], **Marco V. Perez, MD**[‖], **Euan A. Ashley, MD, PhD**[‖], **Vladimir Yarov-Yarovoy, PhD**[§], **Ebenezer N. Yamoah, PhD**[†], **Xiao-Dong Zhang, PhD**[*,‡], **Nipavan Chiamvimonvat, MD**[*,‡]

[*] Division of Cardiovascular Medicine, Department of Internal Medicine, University of California, Davis, Davis, California

[†] Department of Physiology and Cell Biology, University of Nevada, Reno, Reno, Nevada

[‡] Department of Veterans Affairs, Northern California Health Care System, Mather, California

[§] Department of Physiology and Membrane Biology, University of California, Davis, Davis, California

[‖] Division of Cardiovascular Medicine, Department of Medicine, Stanford University, Stanford, California

Abstract

BACKGROUND—Long QT syndrome (LQTS) is a hereditary disease that predisposes patients to life-threatening cardiac arrhythmias and sudden cardiac death. Our previous study of the human *ether-à-go-go* related gene (*hERG*)–encoded K^+ channel ($K_V11.1$) supports an association between hERG and RING finger protein 207 (RNF207) variants in aggravating the onset and severity of LQTS, specifically T613M hERG ($hERG_{T613M}$) and RNF207 frameshift ($RNF207_{G603fs}$) mutations. However, the underlying mechanistic underpinning remains unknown.

OBJECTIVE—The purpose of the present study was to test the role of RNF207 in the function of *hERG*-encoded K^+ channel subunits.

METHODS—Whole-cell patch-clamp experiments were performed in human embryonic kidney (HEK 293) cells and human induced pluripotent stem cell-derived cardiomyocytes (hiPSC-CMs) together with immunofluorescent confocal and high resolution microscopy, auto-ubiquitinylation assays, and co-immunoprecipitation experiments to test the functional interactions between hERG and RNF207.

Address reprint requests and correspondence: Drs Nipavan Chiamvimonvat and Xiao-Dong Zhang, Division of Cardiovascular Medicine, Department of Medicine, University of California, Davis, 451 Health Science Drive, GBSF 6315, Davis, CA 95616. nchiamvimonvat@ucdavis.edu and xdzhang@ucdavis.edu.

[1]Equal contributions.

Disclosures: The authors have no conflicts of interest to disclose.

Appendix

Supplementary data

Supplementary data associated with this article can be found in the online version at https://doi.org/10.1016/j.hrthm.2021.10.005.

RESULTS—Here, we demonstrated that RNF207 serves as an E3 ubiquitin ligase and targets misfolded $hERG_{T613M}$ proteins for degradation. $RNF207_{G603fs}$ exhibits decreased activity and hinders the normal degradation pathway; this increases the levels of $hERG_{T613M}$ subunits and their dominant-negative effect on the wild-type subunits, ultimately resulting in decreased current density. Similar findings are shown for $hERG_{A614V}$, a known dominant-negative mutant subunit. Finally, the presence of $RNF207_{G603fs}$ with $hERG_{T613M}$ results in significantly prolonged action potential durations and reduced hERG current in human-induced pluripotent stem cell–derived cardiomyocytes.

CONCLUSION—Our study establishes RNF207 as an interacting protein serving as a ubiquitin ligase for *hERG*-encoded K^+ channel subunits. Normal function of RNF207 is critical for the quality control of hERG subunits and consequently cardiac repolarization. Moreover, our study provides evidence for protein quality control as a new paradigm in life-threatening cardiac arrhythmias in patients with LQTS.

Keywords

Cardiac ion channels; E3 ubiquitin ligase; Endoplasmic reticulum-associated degradation; Human *ether a-go-go related* gene (*hERG*)–encoded potassium channels; Human induced pluripotent stem cells; Human induced pluripotent stem cell-derived cardiomyocytes; Long QT syndrome; Protein quality control; RING finger protein 207 (RNF207)

Introduction

The pore-forming α subunit of the $K_v11.1$ channel (human *ether-à-go-go related* gene [hERG], encoded by the *KCNH2* gene) underlies the rapid component of the delayed rectifier K^+ current (I_{Kr}).[1,2] The *hERG*-encoded K^+ channel is known to play a critical role in ventricular repolarization. Loss-of-function mutations in *hERG*-encoded K^+ channels result in decreased I_{Kr}, delayed repolarization, and the prolonged QT interval characteristic of long QT syndrome (LQTS) type 2.[3,4]

Genetic mutations in cardiac ion channels, collectively known as *cardiac ion channelopathies*, have been shown to cause a significant percentage of LQTS cases.[5–8] Currently, it is estimated that 1 in 5000 people carry an LQTS mutation. Defects in *hERG*-encoded K^+ channels are the second leading cause of LQTS. Moreover, *hERG*-encoded K^+ channels represent the most common target for drug-induced LQTS.[1,3,4,9]

Previous studies have provided new evidence that LQTS manifests not only from mutations in cardiac ion channels (as in LQT1, LQT2, and LQT3) but also from mutations in ion channel interacting proteins (such as calmodulin in LQT14–LQT16).[10,11] One potential ion channel interacting protein is RING finger protein 207 (RNF207), encoded by its gene located on chromosome 1. RNF207 is a specialized type of zinc finger protein, shown to be associated with prolongation of the QT interval.[12–14]

Our previous study revealed RNF207 as a potential modifier of the hERG channel.[15] Specifically, a term *female infant* presented with perinatal LQTS with recurrent life-threatening ventricular arrhythmias. Using whole-genome sequencing (WGS), a paternally inherited, known pathogenic variant in *KCNH2* leading to a missense mutation (p.T613M,

$hERG_{T613M}$) was identified. In addition, WGS revealed a maternally inherited variant of unknown significance in the *RNF207* gene (a frameshift mutation, $RNF207_{G603fs}$). The patient was heterozygous for both variants; however, neither parent presented with LQTS. The findings suggest that the patient's presentation of LQTS may result from the simultaneous inheritance of the heterozygous RNF207 variant with the $hERG_{T613M}$ channel (Figure 1A).

Previous literature has shown that the T613M hERG mutation ($hERG_{T613M}$, located in the CpG sequence of the pore helix, Figure 1A) produces no detectable current and very low surface expression, suggesting a trafficking defect.[16] Coexpression of $hERG_{T613M}$ with wild-type hERG ($hERG_{WT}$) subunits presented very low current density, indicating that $hERG_{T613M}$ may exert a dominant-negative effect when forming heterotetramers with the $hERG_{WT}$ subunit.[16] There is evidence for an interaction between $hERG_{WT}$ and RNF207 proteins via RNF207's RING domain.[12] This RING domain, as well as RNF207's structural similarity to tripartite motif-containing proteins, suggests a potential function of RNF207 as an E3 ubiquitin ligase and a possible role in facilitating protein degradation.[17] However, the exact molecular mechanisms remain unexplored.

Misfolded proteins are frequently degraded by endoplasmic reticulum (ER)–associated degradation (ERAD).[17–20] After polyubiquitination, proteins are dislocated from the ER and degraded by proteasome within the cytosol. Several quality control proteins targeting *hERG*-encoded K^+ channel subunits have been identified.[20,21] RNF207 has been shown to interact with chaperones heat shock protein, involved in the regulation of hERG subunits.[12,22,23] Therefore, RNF207 may play a critical role in ER-associated degradation.

Here, we demonstrate that RNF207 serves as one of the ubiquitin ligases and targets misfolded $hERG_{T613M}$ proteins for degradation. Mutant RNF207 ($RNF207_{G603fs}$) exhibits decreased activity and hinders the normal degradation pathway; this increases the levels of $hERG_{T613M}$ subunits and their dominant-negative effect on the WT subunits, ultimately resulting in decreased current density. Our study provides novel mechanisms whereby dysfunction in degradation-dependent quality control plays a key role in aggravating the effects of existing LQTS mutations.

Methods

Please see detailed Materials and Methods in the Online Supplement.

Results

$hERG_{T613M}$ exerts a dominant-negative effect when coexpressed with $hERG_{WT}$

Human embryonic kidney 293 cells were transfected with hERG and an accessory subunit, KCNE2 (MiRP1).[24,25] The $hERG_{T613M}$ subunit failed to conduct I_{Kr} because of membrane trafficking defects (Figures 1B and 1D; Online Supplemental Figures 1 and 2), consistent with previous studies.[16] Coexpression of $hERG_{WT}$ with $hERG_{T613M}$ only partially rescued I_{Kr} with significantly reduced current density compared with expression of $hERG_{WT}$ subunits alone (Figures 1B–1D). Moreover, the $hERG_{WT}$:$hERG_{T613M}$ current exhibited

significantly faster time constants for activation and inactivation and significantly slower time constants for deactivation and recovery from inactivation (Figures 1E–1H and Online Supplemental Figure 3), supporting the formation of heterotetramers between WT and mutant subunits.

hERG-encoded K^+ channel subunits colocalize with $RNF207_{WT}$

Immunofluorescence experiments in guinea pig and rabbit ventricular cardiomyocytes showed strong colocalization of hERG and RNF207 proteins as well as colocalization of hERG and RNF207 with α-actinin2, used to mark the z lines (Figure 2A and Online Supplemental Figures 4 and 5). Both hERG and RNF207 proteins localized near the z lines (Figure 2A and Online Supplemental Figure 4C), consistent with the previous literature.[26] We further used proximity ligation assay (PLA), which detects whether 2 proteins of interest are ≤40 nm apart (Figures 2B and 2C).[27] Robust PLA signals were observed in guinea pig ventricular myocytes co-labeled with anti-hERG, anti-RNF207, and anti–α-actinin2 antibodies (Figure 2B and Online Supplemental Movie 1). In contrast, PLA signals were completely absent when one of the primary antibodies was omitted (Figure 2C). The results further support a close association (≤40 nm) between *hERG*-encoded K^+ channel subunits and RNF207.

$RNF207_{G603fs}$ exhibits decreased E3 ubiquitin ligase activity

Using an auto-ubiquitinylation assay, we demonstrated that RNF207 is, indeed, an E3 ubiquitin ligase (Figure 2D). Compared with the known auto-ubiquitin ligase MDM2, $RNF207_{WT}$ displayed strong auto-ubiquitinylation (Figure 2D). In the presence of $hERG_{WT}$, we did not observe significant ubiquitination by $RNF207_{WT}$ (Figure 2E, lane 2). In contrast, incubation of $RNF207_{WT}$ with $hERG_{T613M}$ resulted in significant ubiquitination of $hERG_{T613M}$ subunits (Figure 2E, lane 3). Importantly, $RNF207_{G603fs}$ failed to tag the $hERG_{T613M}$ mutant subunit with ubiquitin (Figure 2E, lane 5, and Figure 2F).

$RNF207_{WT}$ decreases the $hERG_{T613M}$ membrane bound population

Hemagglutinin (HA) and c-Myc tags were inserted into the S1-S2 linker of $hERG_{WT}$ and $hERG_{T613M}$, respectively, in order to quantify the ratio of hERG subunits on the membrane vs those in the cytosol (nonpermeabilized to permeabilized fluorescence ratios, Figures 3A and 3B).[28] $hERG_{T613M}$ subunits failed to show fluorescence signals under nonpermeabilized conditions (Figure 3A). The $hERG_{WT}$:$hERG_{T613M}$ group, however, showed normal fluorescent levels.

When $hERG_{WT}$:$hERG_{T613M}$:$RNF207_{WT}$ were coexpressed (Figures 3A and 3C), $hERG_{WT}$-HA showed normal fluorescence on the membrane, whereas $hERG_{T613M}$-Myc was primarily seen in the cytosol (Figures 3A and 3C). The addition of $RNF207_{G603fs}$, however, resulted in an increase in $hERG_{T613M}$ subunits on the membrane, suggesting decreased degradation of hERGT613M by RNF207G603fs.

$RNF207_{WT}$ increases the degradation of $hERG_{T613M}$ subunits

Brefeldin A, an inhibitor of ER-to-Golgi transport, decreased the fully glycosylated 155 kDa form, while the cytosolic core glycosylated 135 kDa form of hERG subunits increased

over time (Figure 4A). There was a significant accumulation of hERG subunits when $hERG_{WT}$:$hERG_{T613M}$ subunits were coexpressed with $RNF207_{WT}$:$RNF207_{G603fs}$ (closed Δ) compared with coexpression with $RNF207_{WT}$ (closed O) (Figures 4A and 4B). The differences between these 2 groups were reduced by MG 132, a proteasome inhibitor, suggesting that $RNF207_{WT}$ may function through the ubiquitin proteasome system (Figures 4A and 4C). Similar effects were also seen with bafilomycin A1, a lysosome inhibitor, suggesting an additional role of lysosomal degradation (Figures 4A and 4D).

RNF207 interacts with hERG K^+ channel subunits via the C terminus

Co-immunoprecipitation experiments revealed that $hERG_{WT}$ or $hERG_{T613M}$ successfully immunoprecipitated $RNF207_{WT}$, suggesting that the 2 proteins form multiprotein complexes (Figure 5A). $RNF207_{G603fs}$ showed a weaker interaction with $hERG_{WT}$, but also interacted with $hERG_{T613M}$.

We designed 4 additional hERG-HA constructs: hERGΔN, hERG ΔC, hERG N terminus, and hERG C terminus (Figure 5B). We coexpressed $RNF207_{WT}$-FLAG with the hERG fragments to determine the interaction domain of the hERG channel with RNF207 (Figure 5C). The lysate samples are shown in lanes 1–4. hERG ΔN and hERG C terminus were able to successfully immunoprecipitate $RNF207_{WT}$ (Figure 5C, upper panel, lanes 5 and 8), while hERG ΔC and hERG N terminus failed to pull down RNF207 (Figure 5C, upper panel, lanes 6 and 7). The reverse experiments were performed in the lower panel. There are some nonspecific bands from the immunoprecipitated samples (Figure 5C, lower panel, lanes 5–8); however, a distinct band of the expected size could be discerned in lane 5, corresponding to $hERG_{WT}$ ΔN. The data suggest that the C terminus of $hERG_{WT}$ plays an important role in its interaction with $RNF207_{WT}$.

To determine the mechanistic underpinning of $hERG_{T613M}$ on the alterations in the time-dependent kinetics of the channel (Figures 1E–1H), we took advantage of the published cryogenic-electron microscopy (cryo-EM) of the hERG structure[29] using *Rosetta modeling* software (Figure 5D). The hERG backbone is shown with the rainbow color scheme from the N terminus (*blue*) to the C terminus (*red*). The T613 residue is seen to position near the extracellular side of the pore, which likely plays critical roles in channel activation and inactivation kinetics as demonstrated in Figures 1E–1H.

$RNF207_{G603fs}$ decreases the I_{Kr} density

Expression of $hERG_{WT}$ with $RNF207_{WT}$ exhibited the normal hERG current density (Figures 6A–6C, black traces). Although $hERG_{T613M}$ and $hERG_{WT}$ coexpression produces very low current density with altered kinetics (Figures 1B–1F), the addition of $RNF207_{WT}$ rescued the current density to near $hERG_{WT}$ levels (Figures 6A–6C, red traces), suggesting the enhanced degradation and subsequent decrease in dominant-negative effects from $hERG_{T613M}$ subunits. Additionally, the time- and voltage-dependent kinetics were restored to near $hERG_{WT}$ levels (Figures 6D–6G), consistent with the notion that the functional channels consist of mostly $hERG_{WT}$ subunits in the form of homotetramers instead of heterotetramers as in Figures 1E–1H. In contrast, $RNF207_{G603fs}$ failed to restore the current density, despite the coexpression with $RNF207_{WT}$ (Figures 6A–6C, blue traces). The

rectification also decreased (Figure 6B). The time constants of recovery from inactivation (closed Δ, Figure 6E) and the slow component of deactivation (open Δ, Figure 6G) were significantly slower in the presence of $RNF207_{G603fs}$, while the activation time constant was significantly faster (Figure 6F).

To further evaluate whether the $RNF207_{G603fs}$ variant may affect the other known dominant-negative hERG mutant subunit, we generated the $hERG_{A614V}$ mutant subunit, a known dominant-negative subunit[30] (Online Supplemental Figure 6). Expression of $hERG_{WT}$ with $RNF207_{WT}$ exhibited normal hERG current density (Online Supplemental Figures 6A–6C, black traces). In contrast, cells expressing $hERG_{WT}$:$hERG_{T613M}$:$RNF207_{WT}$:$RNF207_{G603fs}$ showed a significantly reduced current density (Online Supplemental Figures 6A–6C, blue traces). Coexpression of $hERG_{WT}$ and $hERG_{A614V}$ with $RNF207_{WT}$ rescued the abnormal current (Online Supplemental Figures 6A–6C, red traces), suggesting that RNF207 serves as a quality control mechanism for LQT2 that is applicable to other *KCNH2* variants.

Coexpression of $hERG_{T613M}$ and $RNF207_{G603fs}$ in human-induced pluripotent stem cell–derived cardiomyocytes results in prolonged action potential durations and a significant decrease in E-4031–sensitive currents

We took advantage of human-induced pluripotent stem cell–derived cardiomyocytes (hiPSC-CMs, iCell, FUJIFILM Cellular Dynamics, Inc., Madison, WI) as a platform (Figures 7A–7F). Cells expressing $hERG_{WT}$:$hERG_{T613M}$:$RNF207_{WT}$:$RNF207_{G603fs}$ (denoted as the “mutant” group) showed significantly longer action potential durations at 50% and 90% repolarization compared with cells expressing $hERG_{WT}$:$RNF207_{WT}$ (WT group) or nontransfected cells (Figures 7A–7C). More importantly, expression of $RNF207_{WT}$ resulted in the “rescue” of delayed repolarization in the mutant group ($hERG_{WT}$:$hERG_{T613M}$:$RNF207_{WT}$, the “rescue” group), consistent with the findings from Figure 6.

Finally, we recorded the E-4031–sensitive currents from the same 3 groups of hiPSC-CMs as in Figure 8. There was a significant decrease in E-4031–sensitive current in hiPSC-CMs expressing $hERG_{WT}$:$hERG_{T613M}$:$RNF207_{WT}$:$RNF207_{G603fs}$ compared with $hERG_{WT}$:$RNF207_{WT}$. Importantly, expression of $RNF207_{WT}$ resulted in the “rescue” of the E-4031–sensitive hERG current ($hERG_{WT}$:$hERG_{T613M}$:$RNF207_{WT}$).

Discussion

While the majority of LQTS cases are attributed to defects in the ion channels, previous studies have provided new evidence where mutations in ion channel interacting proteins act as potential culprits in the development of LQTS. Calmodulin’s role in LQT14, LQT15, and LQT16 is 1 such example.[10] Here, we propose that quality control mechanisms play a key role in either aggravating or appeasing the existing ion channel mutations.

Protein quality control as a new paradigm for cardiac arrhythmias in LQTS

In our previously published patient,[15] we observed severe LQTS with early onset. WGS identified that the patient was heterozygous for the $hERG_{T613M}$ and $RNF207_{G603fs}$ variants. The absence of LQTS symptoms in the parents suggests that the combination of these

2 mutations may be responsible for aggravating the LQTS phenotype. Our present study suggests that quality control mechanisms, including degradation by ubiquitin ligases such as RNF207, are critically important in regulating the impacts of these ion channel mutations. Indeed, we demonstrated that $RNF207_{WT}$ rescued the detrimental effects of $hERG_{T613M}$ coexpression with $hERG_{WT}$ while the addition of $RNF207_{G603fs}$ failed to rescue I_{Kr} and aggravate the LQTS phenotype. Our results support the underlying hypothesis that quality control mechanisms are critical regulators of ion channel function and consequently disorders such as LQTS and sudden cardiac death.

Identification of RNF207 as an E3 ubiquitin ligase

We demonstrated that RNF207 colocalizes with the hERG channel, near the z lines, in ventricular cardiomyocytes. We confirmed that $RNF207_{WT}$ functions as an E3 ubiquitin ligase for $hERG_{T613M}$, primarily through the ubiquitin proteasome system. Co-immunoprecipitation experiments confirm that RNF207 and hERG reside within the same multiprotein complex. $RNF207_{WT}$ successfully rescues the hERG current density via ubiquitination when WT and mutant subunits are coexpressed, whereas $RNF207_{G603fs}$ fails to ubiquitinate and rescue I_{Kr}.

Functional roles of T613 residues in the time-dependent kinetics of hERG channels

Previous literature has shown that $hERG_{T613M}$ fails to traffic and produce currents when expressed alone but exhibits decreased current density when coexpressed with $hERG_{WT}$, consistent with our findings.[17] Additionally, $hERG_{T613M}$, when coexpressed with $hERG_{WT}$, alters the time- and voltage-dependent kinetics. Specifically, the activation and inactivation time constants are significantly faster while the deactivation and recovery from inactivation are significantly slower when $hERG_{T613M}$ and $hERG_{WT}$ are coexpressed. The changes in inactivation are in accordance with our molecular model of $hERG_{T613M}$, as the rectification from the hERG channel's inactivation process has been shown to be similar to C-type inactivation, which takes place near the outer region of the pore helix.[31]

Findings from hiPSC-CMs show the unexpected effects of mutant subunits on the diastolic potentials. Future studies are required to explore other K^+ currents including inwardly rectifying K^+ current (I_{K1}) that may contribute to the observed findings.

Findings from previous studies

Previous genome-wide association studies have identified single nucleotide polymorphisms within the gene encoding RNF207 and QT interval prolongation.[12–14] Our findings are consistent with a previous study showing that RNF207 and the *hERG*-encoded K^+ channel interact and colocalize.[12] The previous study suggests that RNF207 overexpression significantly increases hERG protein trafficking, membrane expression, and the current density. Our present study provides additional evidence for a novel role of RNF207 as a channel interacting partner that serves critical roles in the quality control of the proteins.

Conclusion

New knowledge of the intricate and precise regulatory mechanisms of ion channels will provide an enormous opportunity to uncover new therapeutic targets that may serve to "fine-tune" ion channel function, instead of "blocking" ion channels directly as in our current forms of antiarrhythmic drugs, thus serving as a paradigm shift in our new rationale for the development of antiarrhythmic therapy.

Supplementary Material

Refer to Web version on PubMed Central for supplementary material.

Acknowledgments

Funding sources: This study was supported in part by a predoctoral fellowship from the National Institutes of Health (NIH)/National Heart, Lung, and Blood Institute Institutional Training Grant NIH T32 HL086350 and NIH F31 HL136120 predoctoral awards (to Dr Ledford); the American Heart Association (AHA) Predoctoral Fellowship Award (to Dr Ren); NIH F32 HL149288 (to Dr Thai); NIH R56 HL138392 (to Dr Zhang); NIH R01 HL085727, NIH R01 HL085844, and NIH R01 HL137228 (to Dr Chiamvimonvat); NIH R01 HL128537 (to Dr Yarov-Yarovoy); VA Merit Review Grant I01 BX000576 and I01 CX001490 (to Dr Chiamvimonvat); NIH R01 DC016099, NIH P01 AG051443, and NIH R01 DC015135 (to Dr Yamoah); and AHA Postdoctoral Fellowship Award, Harold S. Geneen Charitable Trust Awards Program for Coronary Heart Disease Research, and AHA Career Development Award (to Dr Sirish). Dr Chiamvimonvat is the holder of the Roger Tatarian Endowed Professorship in Cardiovascular Medicine. Molecular graphics and analyses were performed with UCSF Chimera (NIH P41 GM103311).

References

1. Sanguinetti MC, Jiang C, Curran ME, Keating MT. A mechanistic link between an inherited and an acquired cardiac arrhythmia: HERG encodes the IKr potassium channel. Cell 1995;81:299–307. [PubMed: 7736582]
2. Trudeau MC, Warmke JW, Ganetzky B, Robertson GA. HERG, a human inward rectifier in the voltage-gated potassium channel family. Science 1995;269:92–95. [PubMed: 7604285]
3. Sanguinetti MC, Tristani-Firouzi M. hERG potassium channels and cardiac arrhythmia. Nature 2006;440:463–469. [PubMed: 16554806]
4. Vandenberg JI, Perry MD, Perrin MJ, Mann SA, Ke Y, Hill AP. hERG K^+ channels: structure, function, and clinical significance. Physiol Rev 2012;92:1393–1478. [PubMed: 22988594]
5. Schwartz PJ, Ackerman MJ, George AL Jr, Wilde AA. Impact of genetics on the clinical management of channelopathies. J Am Coll Cardiol 2013;62:169–180. [PubMed: 23684683]
6. Ackerman MJ. The long QT syndrome: ion channel diseases of the heart. Mayo Clin Proc 1998;73:250–269. [PubMed: 9511785]
7. Giudicessi JR, Ackerman MJ. Genotype- and phenotype-guided management of congenital long QT syndrome. Curr Probl Cardiol 2013;38:417–455. [PubMed: 24093767]
8. Kass RS, Moss AJ. Long QT syndrome: novel insights into the mechanisms of cardiac arrhythmias. J Clin Invest 2003;112:810–815. [PubMed: 12975462]
9. Curran ME, Splawski I, Timothy KW, Vincent GM, Green ED, Keating MT. A molecular basis for cardiac arrhythmia: HERG mutations cause long QT syndrome. Cell 1995;80:795–803. [PubMed: 7889573]
10. Crotti L, Johnson CN, Graf E, et al. Calmodulin mutations associated with recurrent cardiac arrest in infants. Circulation 2013;127:1009–1017. [PubMed: 23388215]
11. Crotti L, Spazzolini C, Tester DJ, et al. Calmodulin mutations and life-threatening cardiac arrhythmias: insights from the International Calmodulinopathy Registry. Eur Heart J 2019;40:2964–2975. [PubMed: 31170290]

12. Roder K, Werdich AA, Li W, et al. RING finger protein RNF207, a novel regulator of cardiac excitation. J Biol Chem 2014;289:33730–33740. [PubMed: 25281747]
13. Newton-Cheh C, Eijgelsheim M, Rice KM, et al. Common variants at ten loci influence QT interval duration in the QTGEN Study. Nat Genet 2009; 41:399–406. [PubMed: 19305408]
14. Pfeufer A, Sanna S, Arking DE, et al. Common variants at ten loci modulate the QT interval duration in the QTSCD Study. Nat Genet 2009;41:407–414. [PubMed: 19305409]
15. Priest JR, Ceresnak SR, Dewey FE, et al. Molecular diagnosis of long QT syndrome at 10 days of life by rapid whole genome sequencing. Heart Rhythm 2014;11:1707–1713. [PubMed: 24973560]
16. Huang FD, Chen J, Lin M, Keating MT, Sanguinetti MC. Long-QT syndrome-associated missense mutations in the pore helix of the HERG potassium channel. Circulation 2001;104:1071–1075. [PubMed: 11524404]
17. Gong Q, Keeney DR, Molinari M, Zhou Z. Degradation of trafficking-defective long QT syndrome type II mutant channels by the ubiquitin-proteasome pathway. J Biol Chem 2005;280:19419–19425. [PubMed: 15760896]
18. Cui Z, Zhang S. Regulation of the human ether-a-go-go-related gene (hERG) channel by Rab4 protein through neural precursor cell-expressed developmentally down-regulated protein 4–2 (Nedd4–2). J Biol Chem 2013; 288:21876–21886. [PubMed: 23792956]
19. Guo J, Wang T, Li X, Shallow H, et al. Cell surface expression of human ether-a-go-go-related gene (hERG) channels is regulated by caveolin-3 protein via the ubiquitin ligase Nedd4–2. J Biol Chem 2012;287:33132–33141. [PubMed: 22879586]
20. Foo B, Williamson B, Young JC, Lukacs G, Shrier A. hERG quality control and the long QT syndrome. J Physiol 2016;594:2469–2481. [PubMed: 26718903]
21. Iwai C, Li P, Kurata Y, et al. Hsp90 prevents interaction between CHIP and HERG proteins to facilitate maturation of wild-type and mutant HERG proteins. Cardiovasc Res 2013;100:520–528. [PubMed: 23963841]
22. Ficker E, Dennis AT, Wang L, Brown AM. Role of the cytosolic chaperones Hsp70 and Hsp90 in maturation of the cardiac potassium channel HERG. Circ Res 2003;92:e87–e100. [PubMed: 12775586]
23. Walker VE, Wong MJ, Atanasiu R, Hantouche C, Young JC, Shrier A. Hsp40 chaperones promote degradation of the HERG potassium channel. J Biol Chem 2010;285:3319–3329. [PubMed: 19940115]
24. Abbott GW. The KCNE2 K^+ channel regulatory subunit: ubiquitous influence, complex pathobiology. Gene 2015;569:162–172. [PubMed: 26123744]
25. Liu L, Tian J, Lu C, et al. Electrophysiological characteristics of the LQT2 syndrome mutation KCNH2-G572S and regulation by accessory protein KCNE2. Front Physiol 2016;7:650. [PubMed: 28082916]
26. Pond AL, Scheve BK, Benedict AT, et al. Expression of distinct ERG proteins in rat, mouse, and human heart: relation to functional I(Kr) channels. J Biol Chem 2000;275:5997–6006. [PubMed: 10681594]
27. Syed AU, Reddy GR, Ghosh D, et al. Adenylyl cyclase 5-generated cAMP controls cerebral vascular reactivity during diabetic hyperglycemia. J Clin Invest 2019;129:3140–3152. [PubMed: 31162142]
28. Rafizadeh S, Zhang Z, Woltz RL, et al. Functional interaction with filamin A and intracellular Ca^{2+} enhance the surface membrane expression of a small-conductance Ca^{2+}-activated K^+ (SK2) channel. Proc Natl Acad Sci U S A 2014;111:9989–9994. [PubMed: 24951510]
29. Wang W, MacKinnon R. Cryo-EM structure of the open human ether-à-go-go-related K^+ channel hERG. Cell 2017;169:422–430.e410. [PubMed: 28431243]
30. Nakajima T, Furukawa T, Tanaka T, et al. Novel mechanism of HERG current suppression in LQT2: shift in voltage dependence of HERG inactivation. Circ Res 1998;83:415–422. [PubMed: 9721698]
31. Spector PS, Curran ME, Zou A, Keating MT, Sanguinetti MC. Fast inactivation causes rectification of the I_{Kr} channel. J Gen Physiol 1996; 107:611–619. [PubMed: 8740374]

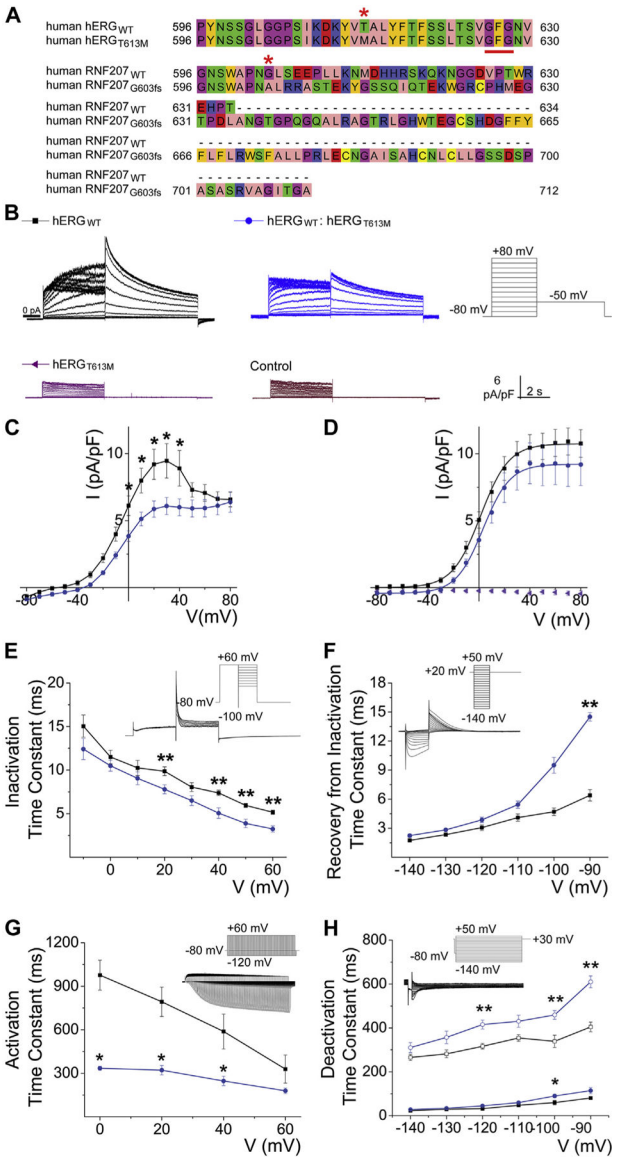

Figure 1.

A Dominant-negative effect and altered channel gating kinetics by $hERG_{T613M}$. **A**: Amino acid sequence alignments for $hERG_{WT}$ and $hERG_{T613M}$ (residues 596–630) and $RNF207_{WT}$ and $RNF207_{G603fs}$ (residue 596 to the end of the polypeptide). The conserved selectivity filter of the hERG subunit GFG is underlined. The asterisk indicates mutated residues (613 in the hERG sequence and 603 in the RNF207 sequence). **B:** Representative recordings from HEK 293 cells expressing hERGWT alone, hERGWT:hERGT613M, hERGT613M alone, or nontransfected cells. **C:** Summary data of current densities for hERGWT alone (*black traces*) compared with $hERG_{WT}$:$hERG_{T613M}$ (*blue traces*). n = 20–30 cells; $*P < .05$. **D:** Summary data for voltage-dependent activation using the peak tail current density fitted using the Boltzmann function (see Online Supplemental Table 1). **E–H:** Time constants of inactivation, recovery from inactivation, activation, and deactivation, respectively, from $hERG_{WT}$ alone (*black traces*) compared with $hERG_{WT}$:$hERG_{T613M}$ (*blue traces*). The insets

show voltage-clamp protocols and representative current traces. n = 6–11 for inactivation; n = 9–11 for recovery from inactivation; n = 3 for activation; n = 5–10 for deactivation. *P < .05, **P < .01. Data shown are mean ± SEM. Analyses were performed using the Student *t* test. Expanded current traces in insets in panels E–H are shown in Online Supplemental Figure 3. ANOVA = analysis of variance; HEK 293 = human embryonic kidney 293; hERG = *human ether-à-go-go* related gene; I = current; ms = millisecond; mV = millivolt; pA/pF = picoampere per picofarad; RNF207 = ring finger protein 207; s = second; SEM = standard error of the mean; V = voltage; WT = wild-type.

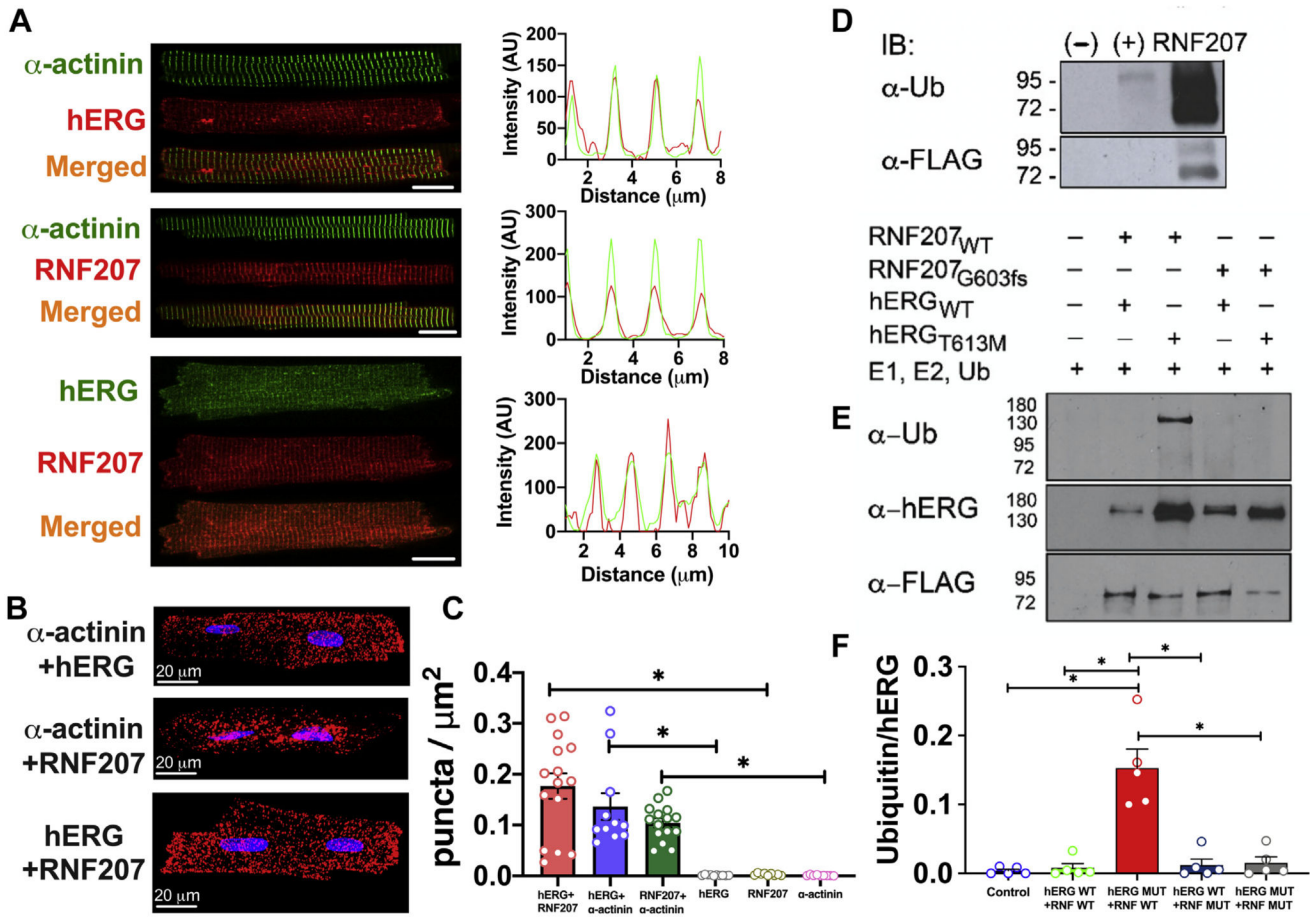

Figure 2.

Colocalization of hERG and RNF207 in guinea pig ventricular cardiomyocytes. **A:** Confocal images showing colocalization among α-actinin2, hERG K^+ channel subunits, and RNF207. Scale bar = 10 μm. The right panels show the corresponding fluorescence intensity profiles perpendicular to the z lines. **B:** Proximity ligation assay (PLA) for α-actinin2, hERG K^+ channel subunits, and RNF207. **C:** Quantification of PLA signals per cell area (puncta/μm^2). n = 15, 11, 15, 10, 9, and 9 cells from left to right bars; *$P < .05$. **D:** Auto-ubiquitinylation assay for $RNF207_{WT}$ (lane 3, right) vs negative control (lane 1, left) and MDM2, a known E3 ubiquitin ligase (positive control, lane 2). Transfected HEK 293 cells were immunoprecipitated (IP) for RNF207-FLAG. An auto-ubiquitinylation assay was conducted on isolated protein, followed by SDS-PAGE and Western blot analysis (IB). Proteins were incubated in the presence of E1 and E2 ubiquitin enzymes, ubiquitin, and ATP. **E:** Ubiquitination assays. Ubiquitinated proteins were absent in the negative control (lane 1). The E3-ubiquitin band appeared for $hERG_{T613M}$ incubated with $RNF207_{WT}$ (lane 3), but not in the presence of $RNF207_{G603fs}$ (lane 5) or with $hERG_{WT}$ subunits (either with $RNF207_{WT}$ [lane 2] or with $RNF207_{G603fs}$ [lane 4]). **F:** Quantification of the data from panel E. n = 5 independent experiments for each group; *$P < .05$. Data shown are mean ± SEM. Analyses were performed using 1-way analysis of variance (ANOVA) with Brown-Forsythe post hoc analyses. AU = arbitraty units; HEK 293 = human embryonic kidney 293; hERG = human *ether-à-go-go* related gene; RNF207 = ring finger protein 207; SDS-PAGE = sodium

dodecyl sulfate-polyacrylamide gel electrophoresis; SEM = standard error of the mean; Ub = ubiquitin; WT = wild-type.

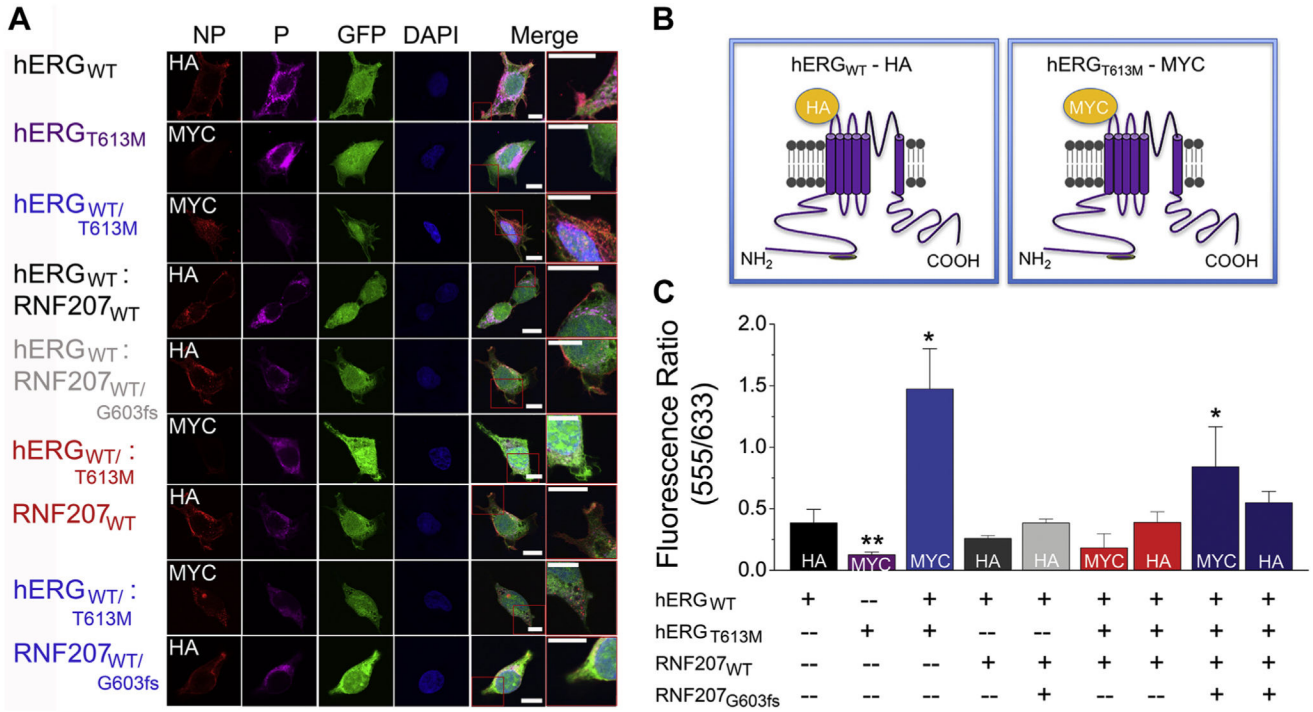

Figure 3.

Surface membrane and cytosolic expression of hERG K^+ channel subunits after coexpression with $RNF207_{WT}$ vs $RNF207_{G603fs}$. **A:** Immunofluorescence confocal microscopic imaging of HEK 293 cells transfected with different combinations of $hERG_{WT}$, $hERG_{T613M}$, $RNF207_{WT}$, and $RNF207_{G603fs}$. NP = nonpermeabilized; P = permeabilized. Scale bar = 10 μm). The last panel in each row represents a higher magnification image from the merged image as outlined in a *red box*. **B:** Schematic diagrams of $hERG_{WT}$-HA and $hERG_{T613M}$-Myc fusion constructs. **C:** Summary data of the fluorescence ratios (555 nm/633 nm). n = 6–10 cells; $*P < .05$, $**P < .01$. Data shown are mean ± SEM. Analyses were performed using ANOVA with Tukey's post hoc analyses. ANOVA = analysis of variance; DAPI = 4'6-diamidino-2-phenylindole; GFP = green fluorescent protein; HA = hemagglutinin; HEK 293 = human embryonic kidney 293; hERG = human *ether-à-go-go* related gene; RNF207 = ring finger protein 207; SEM = standard error of the mean; WT = wild-type.

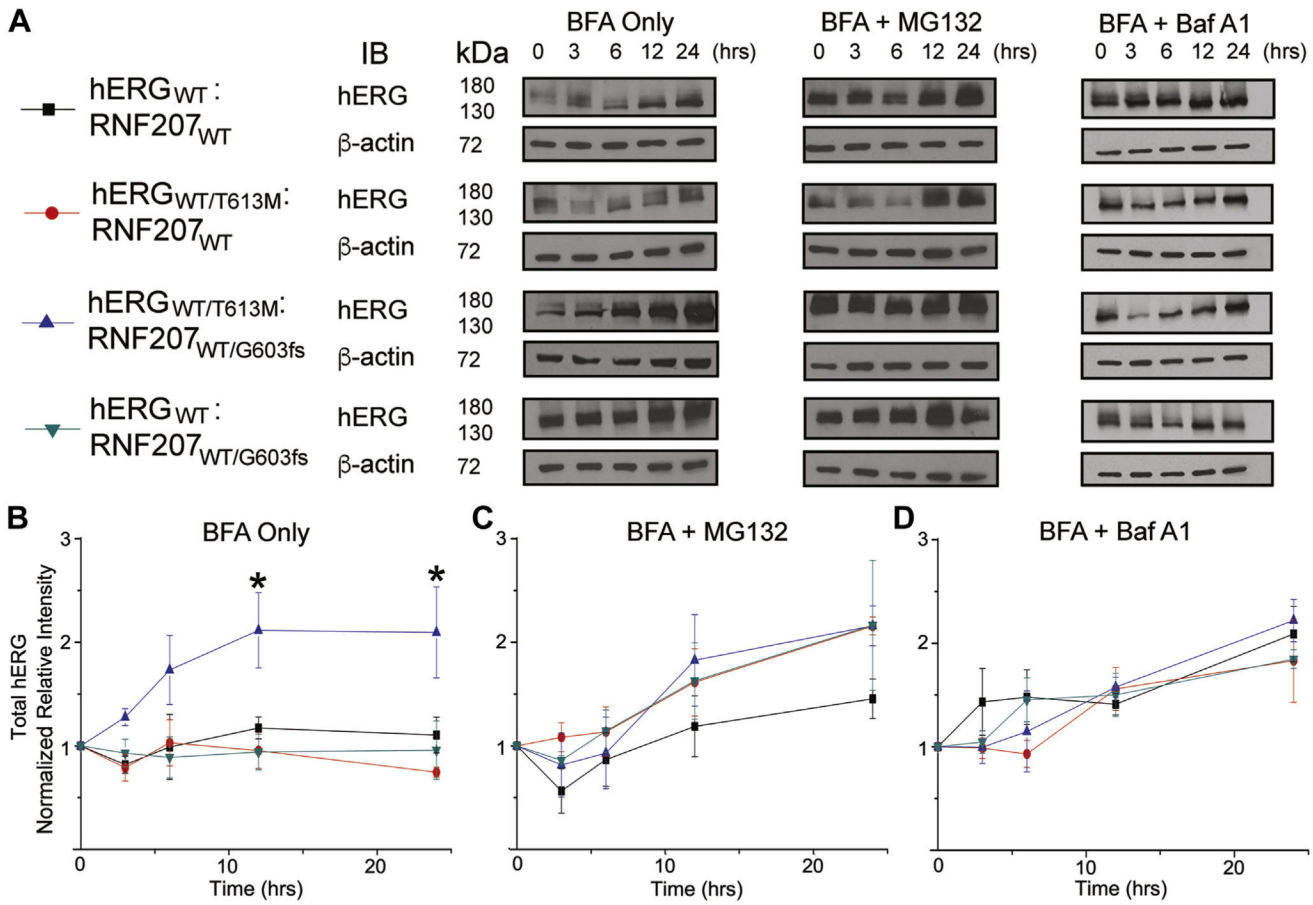

Figure 4.

Distinct effects of RNF207$_{WT}$ vs RNF207$_{G603fs}$ on the degradation of hERG K^+ channel subunits. **A:** Degradation assay for HEK 293 cells collected before (time = 0) vs 3, 6, 12, and 24 hours after treatment. Cells were treated with brefeldin A (left panel), brefeldin A + MG 132 (middle panel), or brefeldin A + bafilomycin A1 (Baf A1; right panel). **B–D:** Summary data from panel A. **P* < .05 in panel B. Data shown are mean ± SEM. n = 5 different independent experiments; **P* < .05. Analyses were performed using ANOVA with Tukey's post hoc analyses. ANOVA = analysis of variance; Baf A1 = bafilomycin A1; BFA = brefeldin A; HEK 293 = human embryonic kidney 293; hERG = human *ether-à-go-go* related gene; IB = immunoblot; kDa = kilodaltons; RNF207 = ring finger protein 207; SEM = standard error of the mean; WT = wild-type.

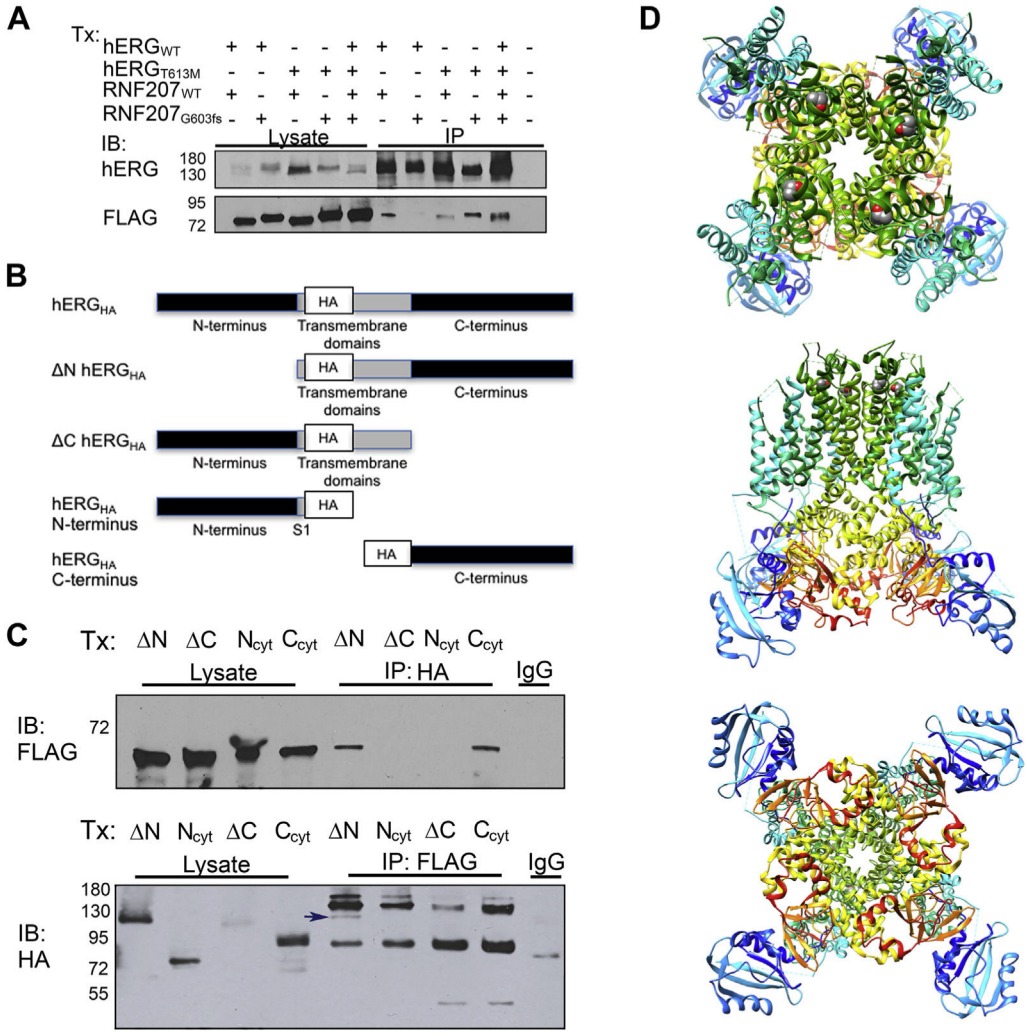

Figure 5.

Multiprotein complexes formed by hERG K^+ channel subunits and RNF207. **A:** Transfected (T_x) HEK 293 cells were immunoprecipitated (IP) using anti-hERG antibody, and Western blot analysis (IB) was performed using anti-hERG and anti-FLAG antibodies to target the RNF207-FLAG fusion protein. Western blot analyses from lysates and IP are shown in lanes 1–5 and lanes 6–10, respectively. The negative control using IgG for IP is shown in lane 11. **B:** Schematic of hERG$_{WT}$ ΔN, hERG$_{WT}$ ΔC, hERG N-terminus, and hERG C-terminus constructs (tagged with HA). **C:** Coimmunoprecipitation of hERG-HA fragments that were cotransfected (Tx) in HEK 293 cells with RNF207$_{WT}$-FLAG. Immunoprecipitation (IP) followed by immunoblotting (IB) was performed using anti-HA (IP:HA, upper panel) and anti-FLAG (IB:FLAG, upper panel) antibodies, respectively. The reverse experiments were conducted as shown in the lower panel. Lanes 1–4 are lysate samples (20 μg each), and lanes 5–8 show immunoprecipitated samples transfected with hERG$_{WT}$ ΔN, hERG$_{WT}$ ΔC, hERG N-terminus, hERG C-terminus, and IgG negative control. Some nonspecific bands are seen in lanes 5–8 in the lower panel. The *blue arrow* in lane 5 in the lower panel shows a band of the expected size for hERG$_{WT}$ ΔN. **D:** *Rosetta* model of hERG (from top to bottom): (1) view from the extracellular side of the membrane, (2) view from the transmembrane side,

and (3) view from the intracellular side of the membrane. The backbone is shown in ribbon representation and colored by the rainbow color scheme from the N terminus (*blue*) to the C terminus (*red*). The side chain of the T613 residue in each subunit is shown using a space filling representation. ANOVA = analysis of variance; cyt = cytosolic; HA = hemagglutinin; HEK 293 = human embryonic kidney 293; hERG = human *ether-à-go-go* related gene; IB = immunoblot; IP = immunoprecipitation; kDa = kilodaltons; RNF207 = ring finger protein 207; SEM = standard error of the mean; Tx = transfection; WT = wild-type.

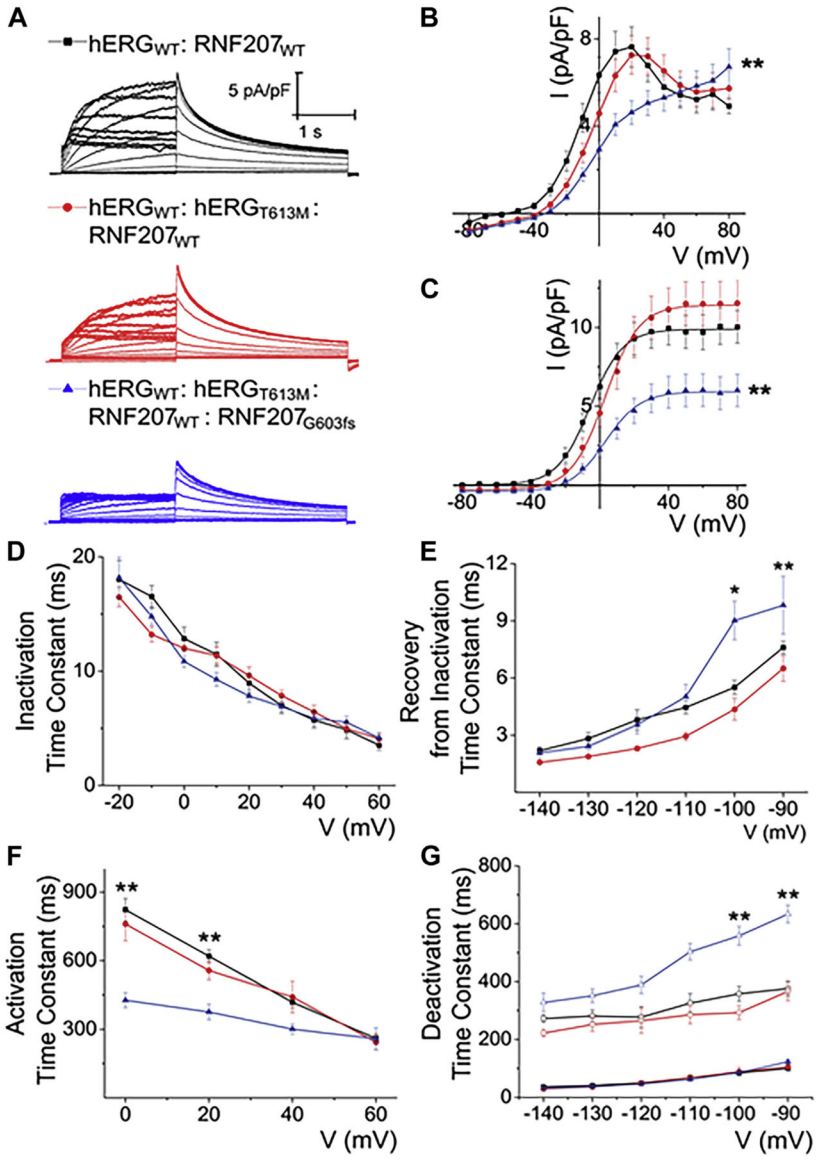

Figure 6.

Differential effects of $RNF207_{WT}$ vs $RNF207_{G603fs}$ on the hERG current. **A:** Representative whole-cell voltage-clamp recordings. **B:** Summary data of current density for $hERG_{WT}$:$RNF207_{WT}$ (*black traces*) compared with $hERG_{WT}$:$hERG_{T613M}$:$RNF207_{WT}$ (*red traces*) and $hERG_{WT}$:$hERG_{T613M}$:$RNF207_{WT}$:$RNF207_{G603fs}$ (*blue traces*). n = 14–19.**C:** Summary data for voltage-dependent activation using the peak tail current density fitted using the Boltzmann function (see Online Supplemental Table 1). **D and E:** Time constants of inactivation and recovery from inactivation for $hERG_{WT}$:$RNF207_{WT}$ (*black traces*) compared with $hERG_{WT}$:$hERG_{T613M}$:$RNF207_{WT}$ (*red traces*) and $hERG_{WT}$:$hERG_{T613M}$:$RNF207_{WT}$:$RNF207_{G603fs}$ (*blue traces*). **F and G:** Time constants for activation and deactivation, where closed Δ, □, and O represent the fast component and open Δ, □, and O represent the slow component of deactivation. n = 5–10 for inactivation; n = 6–12 for recovery from inactivation; n = 3–5 for activation; n =

5–10 for deactivation. *$P < .05$, **$P < .01$. In panels B and C, **$P < .01$ for $hERG_{WT}$:$hERG_{T613M}$:$RNF207_{WT}$:$RNF207_{G603fs}$ compared with $hERG_{WT}$:$RNF207_{WT}$ and $hERG_{WT}$:$hERG_{T613M}$:$RNF207_{WT}$ throughout positive voltages and was shown only at the end of the curves for clarity. Data shown are mean ± SEM. Analyses were performed using ANOVA with Tukey's post hoc analyses. ANOVA = analysis of variance; HEK 293 = human embryonic kidney 293; hERG = human *ether-à-go-go* related gene; RNF207 = ring finger protein 207; SEM = standard error of the mean; WT = wild-type.

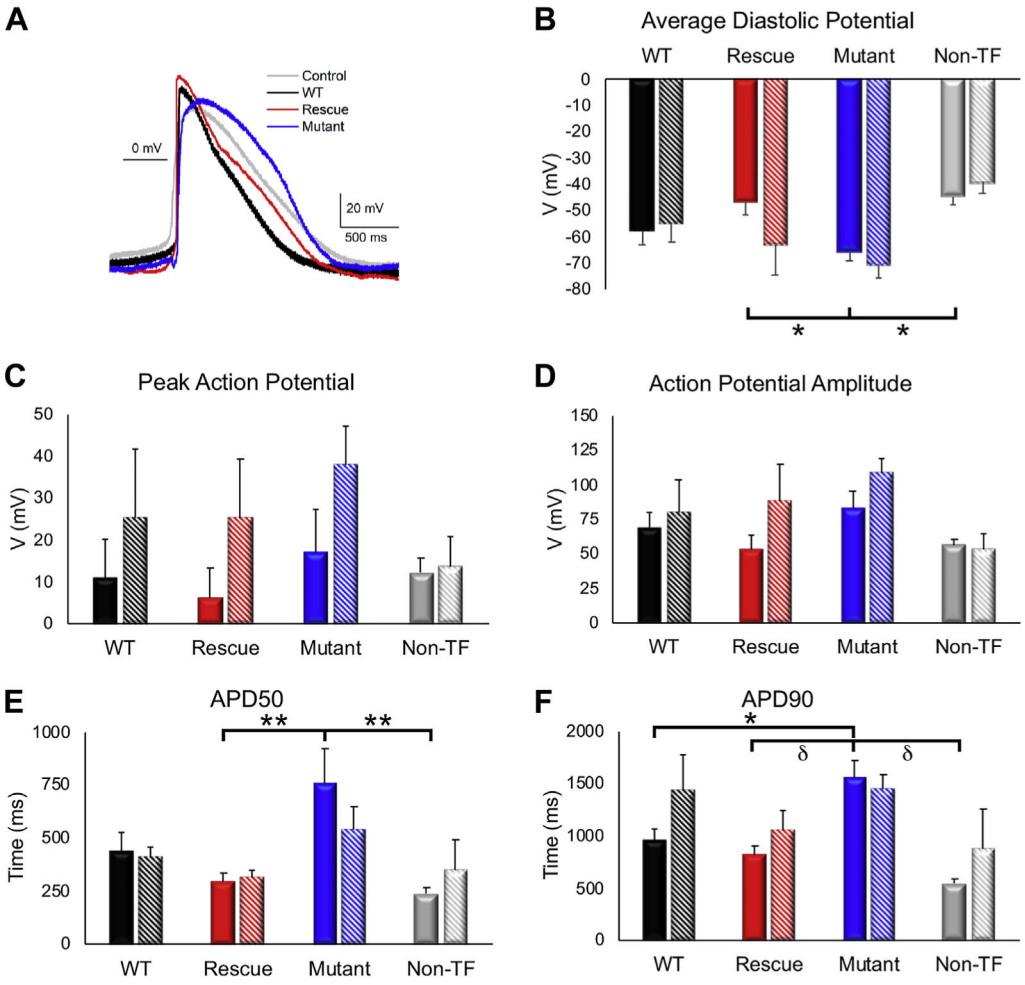

Figure 7.

Regulation of APDs of hiPSC-CMs by RNF207. **A:** Representative action potential recordings (iCell, Cellular Dynamics) in cells expressing $hERG_{WT}$:$RNF207_{WT}$ (*black trace*), $hERG_{WT}$:$hERG_{T613M}$:$RNF207_{WT}$ (*red trace*), and $hERG_{WT}$:$hERG_{T613M}$:$RNF207_{WT}$:$RNF207_{G603fs}$ (*blue trace*) as well as a nontransfected cell (*gray trace*). **B–F:** Summary data for action potential recordings in nontransfected cells (labeled "Non-TF"; *gray bar*) compared with $hERG_{WT}$:$RNF207_{WT}$ (labeled "WT"; *black bar*), $hERG_{WT}$:$hERG_{T613M}$:$RNF207_{WT}$ (labeled "Rescue"; *red bar*), and $hERG_{WT}$:$hERG_{T613M}$:$RNF207_{WT}$:$RNF207_{G603fs}$ (labeled "Mutant"; *blue bar*) at baseline (*solid bars*) vs 1 μM E-4031 (*striped bars*). Data are shown for average diastolic potential (panel B), peak action potential (panel C), action potential amplitude (panel D), action potential duration at 50% repolarization or APD_{50} (panel E), and action potential duration at 90% repolarization or APD_{90} (panel F). Data shown represents the average of 5 action potentials per cell, with n = 6–9 cells for baseline recordings and n = 3–5 cells for E-4031 recordings. **P*<.05, ***P*<.01, §*P*<.001. Data shown are mean ± SEM. Analyses were performed using ANOVA with Tukey's post hoc analyses. ANOVA = analysis of variance; APD = action potential duration; APD50 and APD90 = APD at 50% and 90% repolarization; hERG = human *ether-à-go-go* related gene; hiPSC-CM = human induced

pluripotent stem cell-derived cardiomyocytes; non-TF = nontransfected cells; RNF207 = ring finger protein 207; SEM = standard error of the mean; WT = wild-type.

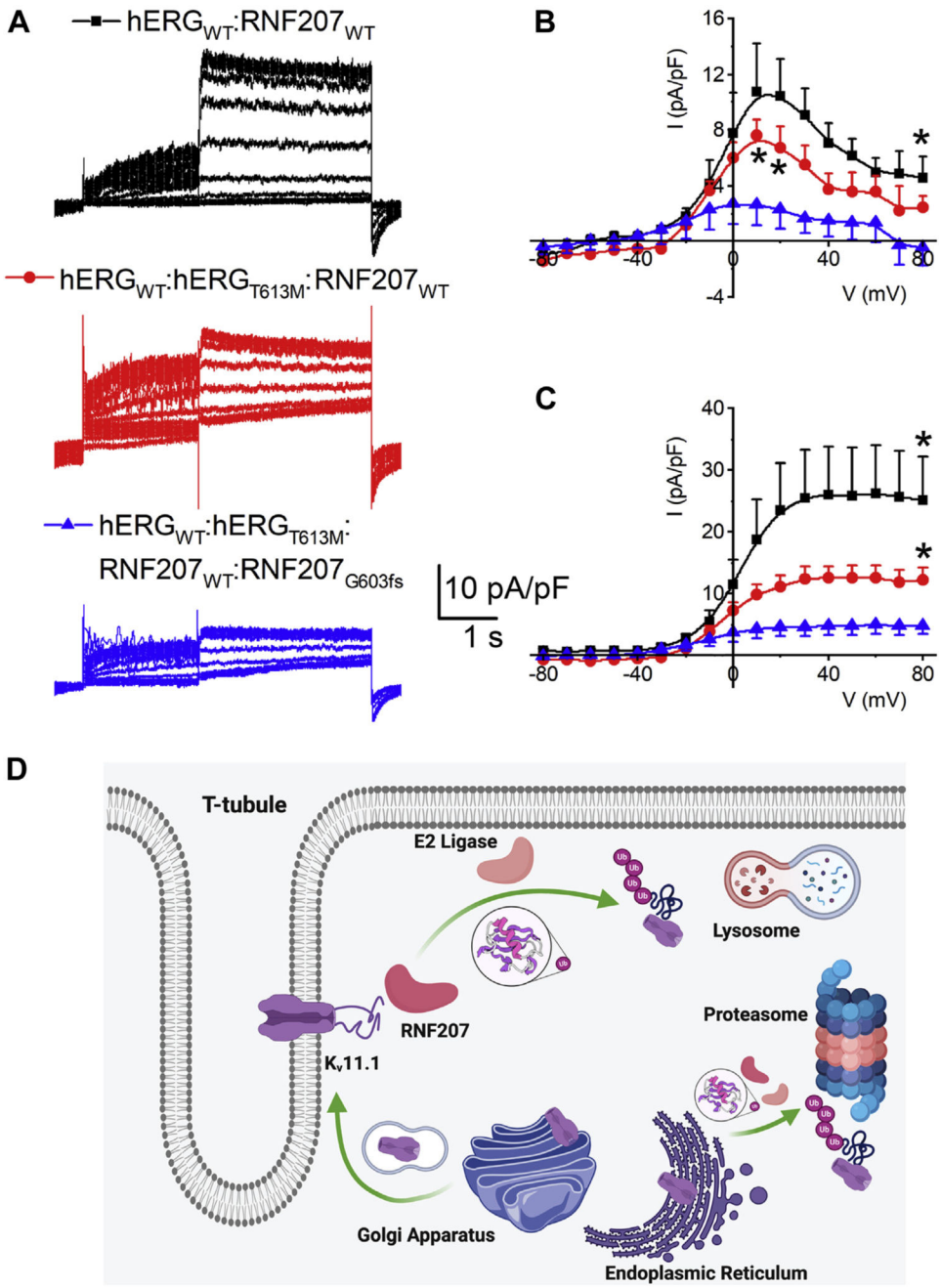

Figure 8.

Regulation of hERG currents by RNF207 in hiPSC-CMs and a schematic diagram of RNF207 interaction with hERG-encoded K^+ channels in adult ventricular myocytes. **A:** Representative E-4031–sensitive currents recorded from hiPSC-CMs expressing hERG$_{WT}$:RNF207$_{WT}$ (*black traces*), hERG$_{WT}$:hERG$_{T613M}$:RNF207$_{WT}$ (*red traces*), and hERG$_{WT}$:hERG$_{T613M}$:RNF207$_{WT}$:RNF207$_{G603fs}$ (*blue traces*). **B:** Summary data of current density for the 3 groups of cells. n = 5–6. **C:** Summary data for voltage-dependent activation using the peak tail current density fitted using the Boltzmann function (see Online Supplemental Table 1). n = 5–6. In panel B, *$P < .05$

for $hERG_{WT}$:$RNF207_{WT}$ compared with $hERG_{WT}$:$hERG_{T613M}$:$RNF207_{WT}$:$RNF207_{G603fs}$ throughout positive voltages and was shown only at the end of the curve for clarity. In panel C, $*P < .05$ for $hERG_{WT}$:$RNF207_{WT}$ and $hERG_{WT}$:$hERG_{T613M}$:$RNF207_{WT}$ compared with $hERG_{WT}$:$hERG_{T613M}$:$RNF207_{WT}$:$RNF207_{G603fs}$ throughout positive voltages and was shown only at the end of the curves for clarity. Analyses were performed using ANOVA with Tukey's post hoc analyses. **D:** Schematic diagram of RNF207 interaction with hERG-encoded K^+ channels ($K_v11.1$) with trafficking and degradation pathways (generated using BioRender, Toronto, Canada). ANOVA 5 analysis of variance; hERG = human *ether-à-go-go* related gene; hiPSC-CM 5 human induced pluripotent stem cell-derived cardiomyocytes; I = current; RNF207 = ring finger protein 207; SEM = standard error of the mean; V = voltage; WT = wild-type.